Photogrammetric Analysis of the Mars Global Surveyor Mapping Data

Jie Shan, Jong-suk Yoon, D. Scott Lee, Randolph L. Kirk, Gregory A. Neumann, and Charles H. Acton

Abstract

This paper studies the photogrammetric mapping properties and capabilities of the Mars Global Surveyor (MGS) mapping data. Starting from the raw MGS data, we decompress the MOC narrow angle images, extract, and calculate their exterior orientation from the SPICE kernels, and calculate the 3D coordinates of MOLA footprints from MOLA PEDR files. A new approach is proposed that registers a MOLA profile to stereo MOC images over the same area with robust and faster convergence. Intersection is conducted to determine the 3D positions of image points measured on MOC stereo pairs. It is shown that there is a nearly constant uncertainty of one MOLA ground spacing distance (approximately 325 m) along the flight direction in MOC and MOLA registration. This is caused by the uncertainties in SPICE kernels, MOLA points, and the determination of time tags for MOC scan lines, which possibly constitutes the dominant error source for the registration. Intersection calculation reaches an optimal balance by distributing the uncertainty evenly in the two images of a stereo pair. As for the photogrammetric mapping capabilities, an uncertainty of 180.8 m in planimetric distance and 30.8 m in elevation difference is estimated. A number of numerical and graphic results over three of the selected candidate landing sites for the Mars Exploration Rover mission are presented for analysis and illustration.

Introduction

A control network is mandatory for Mars topographic surveying which has been a continuous effort over the last three decades. As described by (Davies, *et al.*, 1999), the first Mars control network is calculated by using nearly 3,000 images along with trajectory and pointing data obtained from Mariner 9 and Viking Orbiters. Wu and Schafer (1984) refine and augment the first results by using analytical photogrammetric triangulation. The refined control network is three dimensional (3D) and has been used for the production of numerous Mars topographic products such as geometrically corrected Mars images, e.g., Mosaicked Digital Image Model (MDIM) 1.0 and 2.X (Kirk, *et al.*, 2000; Kirk, *et al.*, 2002b). Zeitler and Oberst (1999) use Pathfinder images to refine a local Mars control network. A combined 3D bundle adjustment reportedly improves the precision to an estimated approximately 740-m in average in each coordinate component for the Pathfinder landing site (Zeitler and Oberst, 1999) and later for the Viking based global control network (Zeitler, *et al.*, 2000).

The next generation of Mars topographic surveying is recently made possible by Mars Global Surveyor (MGS). MGS is a satellite traveling around the Mars in a polar orbit. Its primary mission objectives are to collect data about the Martian surface, atmosphere and magnetic properties, to learn about the Earth by comparing it to Mars and to build a comprehensive dataset for future mission planning (Albee, *et al.*, 2001). The MGS mapping payloads include two types of mapping instruments: a laser altimeter, Mars Orbiter Laser Altimeter (MOLA) and three pushbroom cameras, Mars Orbiter Camera (MOC) including two identical wide angle cameras (MOC WA), one for blue band and one for red band, and one narrow angle panchromatic camera (MOC NA) (Albee, *et al.*, 2001). The mapping-related nominal properties of MGS and its instruments are summarized in Table 1 based on the individual reports from (Albee, *et al.*, 2001; Caplinger and Malin, 2001; Malin and Edgett, 2001; Smith, *et al.*, 2001).

A number of studies on the MGS data processing have been published recently. Following the first reports on MOLA topography (Smith, *et al.*, 1998, 1999), most recent study suggests an approximate 1 m vertical and 100 m horizontal accuracy of MOLA data based on crossover analysis (Neumann, *et al.*, 2001). Finer regional MOLA digital elevation models (DEM) up to $1/256° \times 1/256°$ resolution are being produced by the MOLA scientific team. Such MOLA topography or DEM are used as a control network in many recent studies to reference existing DEM, MDIM, control network, as well as, newly collected MOC images. Diverse results have been reported in early studies. Smith, *et al.* (1998) show local MOLA spots have an approximate 10–20 km displacement in longitude from MDIM images. Muller and Kim (1999), and Kim, *et al.* (2000) report a vertical offset up to 1.8 km between DEM generated from Viking Orbiter images and MOLA data. In a similar effort, Baratoux, *et al.* (2001) register Viking DEM to MOLA data to improve the DEM accuracy. Archinal, *et al.* (2002) present their initial results on improving the existing photogrammetric control network by using MOLA-derived radii and Digital Image Models (DIM) to improve control point absolute radii and horizontal positions.

Despite all these reported discrepancies with previous mapping results, recent investigation suggests good consistency between MOC images and MOLA data. Anderson and

Jie Shan, Jong-suk Yoon, and D. Scott Lee are with Geomatics Engineering, School of Civil Engineering, Purdue University, 550 Stadium Mall Drive, West Lafayette, IN 47907-2051 (jshan@ecn.purdue.edu).

Randolph L. Kirk is with the Astrogeology Team, U.S. Geological Survey, 2255 N. Gemini Drive, Flagstaff, AZ 86001.

Gregory A. Neumann is with the Earth, Atmospheric and Planetary Sciences, Massachusetts Institute of Technology, Cambridge, MA 02139.

Charles H. Acton is with the Jet Propulsion Laboratory, California Institute of Technology, MS 301-125L, 4800 Oak Grove Drive, Pasadena, CA 91109.

Photogrammetric Engineering & Remote Sensing
Vol. 71, No. 1, January 2005, pp. 97–108.

0099-1112/05/7101–0097/$3.00/0

TABLE 1. MAPPING PROPERTIES OF MGS AND ITS INSTRUMENTS

MGS	MOC		MOLA
	Narrow Angle (NA)	Wide Angle (WA)	
–Altitude: ~370-km –Period: ~1.9 hours –Revisit time: ~7 sols (Martian days) –Inclination: 92.9 deg. –Velocity: ~3.4-km/sec	–Spectral: panchromatic 2048 CCD linear array –Focal length: 3500-mm –Ground resolution: ~1.4-m/pixel (nadir) –Field of view: 0.4 deg.	–Spectral: blue and red 3456 CCD linear array –Focal length: 11.3-mm –Ground resolution: ~280-m/pixel (nadir) –Field of view: 140 deg.	–Infrared pulse: 1064-nm –Pulse rate: 10-Hz –Laser spot: 0.4-mrad (~130-m on ground) –Range measurement resolution: ~37.5-cm –Along track ground spacing: ~330-m

Parker (2002), Ivanov and Lorre (2002), Kirk, *et al.* (2001; 2002b), and Soderblom, *et al.* (2002) report on the precision registration between MOC and MOLA data for the selected candidate landing sites for the Mars Exploration Rover (MER) mission (landed in January 2004). The registration is achieved through a refined camera calibration model, instrument calibration parameters, and trial-and-error studies. Using the extracted orientation information of MOC images from Spacecraft, Planet, Instrument, C-matrix, Events (SPICE) kernels (Acton, 1996), Kirk, *et al.* (2002b) generate high resolution DEM over the selected candidate landing sites from MOC NA images. Rosiek, *et al.* (2001) attempt to use high resolution Viking images together with MOC images when their stereo coverage is not available. In addition to DEM, other topographic products can be produced using MGS data. Orthoimages are made over areas of interest using MOLA derived elevation data (Niedermaier, *et al.*, 2002; Wählisch, *et al.*, 2002). The first global image mosaic is produced using MOC WA images as reported by (Caplinger, 2002). A photo-clinometric approach or shape from shading is used by (Anderson and Parker, 2002; Beyer and McEwen, 2002; Kirk, *et al.*, 2002a) to analyze the topographic characteristics of the selected candidate landing sites. Similar analyses are carried out using stereo pairs based on photogrammetric principles (Kirk, *et al.*, 2002b; Ivanov and Lorre, 2002).

The objective of this work is to study the mapping properties and capabilities of the MGS mapping data with focus on their intrinsic consistency and uncertainty. In particular, we investigate the uncertainty of MOC and MOLA registration and the uncertainty of point determination using MOC stereo images. The methodology is summarized as follows. After collecting raw MOC stereo images over the selected study sites, we conduct an exhaustive search to the entire MOLA data sets to find all MOLA profiles including those both simultaneously and non-simultaneously collected with a MOC image that cover the same area as the MOC image. To carry out photogrammetric reduction, the exterior orientation of MOC images is extracted and calculated using SPICE kernels, while the original MOLA records are then processed to obtain the 3D coordinates. An approach based on the rigorous collinearity condition of pushbroom camera is proposed that projects a MOLA 3D point onto MOC images such that a MOLA profile is registered with MOC images. To determine the 3D ground coordinates, a number of conjugate points are measured in MOC stereo pairs, with which the intersection calculation is conducted based on the known MOC position and pointing information. Unlike the existing studies, we register one MOLA profile on both images of a stereo pair, which allows us to discover the uncertainty of the registration by comparing the corresponding image features. The intersection residuals demonstrate the uncertainty of 3D point determination using MOC images. To support our study, both quantitative and graphic results are presented over three study sites, each of which has a stereo MOC image pair and two MOLA profiles. Because of the lower resolution (approximately 280 m/pixel at nadir, see Table 1) of the MOC WA imagery, only MOC NA images (1.4 m/pixel resolution at nadir, see Table 1) are used in this study.

Data Preparation and Preprocessing

The original MGS mapping data are preprocessed and archived by a number of MGS mission teams. These original data and their processing results which hereafter are all referred to as *raw data*, are documented, maintained, and updated by the Navigation and Ancillary Information Facility (NAIF) at the Jet Propulsion Laboratory (JPL) for scientific research uses. For photogrammetric reduction, the first step is to locate, access, and understand all the mapping related data. After that, we process the raw data to derive the information needed for the subsequent photogrammetric mapping reductions.

Data Preparation

This step locates and obtains the data files for the selected study sites from the entire MGS data archive. The data should include MOC images, MOLA range measurements and other records of MOLA profiles, MGS (MOC) positions, MOC pointing angles, and their related metadata. Specifications, calibration parameters of MGS instruments, Mars datum definitions and other information necessary for the subsequent reduction should also be acquired.

Locating the data starts with MOC images and MOLA profiles. We choose three of the candidate landing sites as our study sites. The MOC images listed in (Kirk, *et al.*, 2002b) are used in the study. The longitude and latitude extents of the study sites are used as a window to search the cumulative index of MOC images. Compressed raw MOC images are accessed and decompressed. To find the MOLA profiles that cover the same areas as the MOC images, an exhaustive search is carried out. Instead of using MOC and MOLA acquisition time as a search index, our search is based on geographic extents of the selected study sites. This search strategy enables us to obtain not only the MOLA data simultaneously collected with a MOC image, but also those that were collected from different orbits. The search is carried out by comparing the areocentric latitude and longitude location of each MOLA footprint with a search window of every study site. Every MOLA footprint is tested against all search windows and saved separately if a match is found. In total, 56 MOLA CDs are searched for each window defined by the MOC image extents. Through this process, more than two MOLA profiles from different orbits are found over one MOC image. However, this paper will only present the processing results of simultaneous MOLA profiles which are found by using the Integrated Software for Imagers and Spectrometers (ISIS) package developed by the US Geological Survey (USGS, 2002). Experience in processing multiple (>2) MOLA profiles will be reported elsewhere.

TABLE 2. MOC IMAGES AND MOLA DATA USED IN THE STUDY

Site Name	Eos Chasma		Gusev Crater		Isidis Planitia	
Image Name	E02-02855	E04-01275	E02-00665	E02-01453	E02-01301	E02-02016
Image No.	1	2	1	2	1	2
Emission Angle (deg.)	0.16	17.97	0.2	22.1	13.0	0.2
Acquisition Date and Time	03/31/2001 (18:17:09.41)	05/18/2001 (00:48:12.50)	03/08/2001 (12:52:54.66)	03/17/2001 (18:39:14.26)	03/15/2001 (23:34:57.72)	03/23/2001 (04:17:44.58)
Exposure Time (ms)	1.8078	1.2052	1.4462	1.4462	0.9642	1.4462
Sum factor	3	2	2	2	2	2
Header No. Lines	9856	7424	10496	8960	8064	8064
File Size (H*W)	9856*6 72	7424*1024	10112*1024	8960*1024	7680*1024	7680*1024
MOC GSD(m/pixel)	5.5	4.1	4.4	4.9	3.3	4.4
MOLA Profile Name	ap19215	ap19802	ap18933	ap19043	ap19019	ap19117
No. of MOLA Points	174	76	142	124	71	107
MOLA GSD(m)	305	341	305	341	340	304

—H*W in row File Size is for height*width, where height is along the flight direction.
—GSD: ground spacing distance.

Table 2 lists the properties of MOC images and MOLA profiles used in this study. As shown in Table 2, Eos Chasma, Gusev Crater and Isidis Planitia sites are selected as our study areas. The Image Name starts with the extension mission name, e.g., E02, followed by the image sequential number. The Image Number is a relative index used only for the simplicity of presentation in this paper. The Emission Angle stands for the angle of the camera boresight direction from nadir. The Acquisition Date and Time shows the starting Coordinated Universal Time (UTC) time of image acquisition while the Exposure Time is the exposure time period in milliseconds for one scan line. Onboard resampling (summation) is applied to the original transmitted image data. The Sum Factor shows most images have a down-sampling factor of 2, however, it may vary from image to image. The Header Number Lines is the expected number of lines of the image encoded in the image header file. The actual image file size (after resampling) is shown in the File Size while the first number is the number of rows (along track), and the second number is the number of columns (across track). It should be noted that the actual number of lines may be different from (less than) the one encoded in the MOC image header which indicates that some lines could not be recovered during the decompression process. This may cause certain difficulty when registering MOLA profiles with MOC images. MOC ground spacing distance (GSD) is the MOC image ground resolution in meters per pixel. The facts of the simultaneously collected MOLA profiles are listed in the last three rows in the table. In addition to the MOLA profile name, the number of MOLA points and the average GSD in meters between two adjacent MOLA footprints are listed as well.

The next step is to acquire the data related to MGS position, pointing, and instruments. These data are archived by NAIF and referred hereafter as SPICE kernels for the simplicity of description. The time at which MOC or MOLA data are collected is used as an index to find the corresponding SPICE kernels. The following SPICE kernels are used in our study:

- Leap seconds kernel (LSK)
- Spacecraft clock kernel (SCLK)
- Instrument parameters kernel (IK): instrument parameters for MOC and MOLA
- Orientation kernel (CK): MGS orientation data
- Planet and spacecraft position kernel (SPK): Mars and MGS position data
- Planets and satellites kernel (PCK): planetary datum and constants

To facilitate the understanding, the functions and relationships of the SPICE kernels used in our study are illustrated in Figure 1.

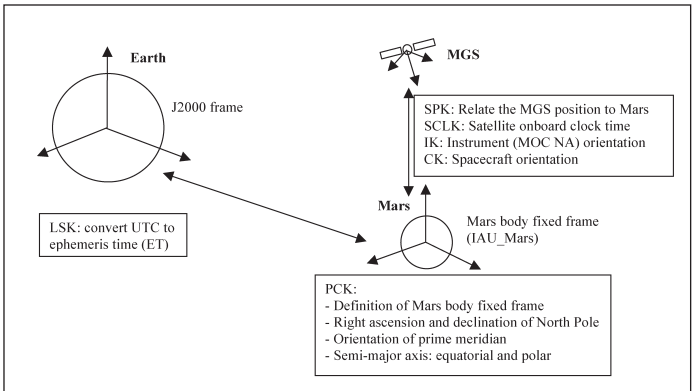

Figure 1. Functions and relationships of the SPICE kernels.

Calculation of MOC Position and Pointing

The exterior orientation (position and pointing) of MOC images needed for photogrammetric reduction is embedded in various SPICE kernels. To obtain this information, MOC time tags for the starting and ending scan lines are first corrected to account for leap seconds and then converted to the ephemeris time (ET). The ET time is used as an index to access the SPICE kernels to obtain the 3D MGS positions under the International Astronomical Union (IAU) 2000 Mars body-fixed coordinate system. A similar procedure is applied to obtain MOC pointing data, however, the ET time needs to be corrected by a bias of −1.15 seconds due to an over-correction when the pointing information in the CK kernel was prepared (NAIF, 2001). The final rotation matrix $\mathbf{R}_{MOC}^{Mars}$ of a MOC scan line relative to the Mars-body fixed frame is a product of two rotation matrices

$$\mathbf{R}_{MOC}^{Mars} = \mathbf{R}_{MGS}^{Mars}\,\mathbf{R}_{MOC}^{MGS}, \tag{1}$$

where $\mathbf{R}_{MGS}^{Mars}$ is the rotation matrix of MGS relative to the Mars-body fixed frame, $\mathbf{R}_{MOC}^{MGS}$ is the one of MOC relative to MGS. Detailed calculation steps can be found in Shan, *et al.* (2002).

It should be noted that one kernel may have different versions or be prepared by different research teams. For kernels with different versions, the latest one at the time of the study is used. Since mapping activities are using IAU 2000 datum (Duxbury, *et al.*, 2002; Seidelmann, *et al.*, 2002), the then-latest PCK kernel (pck00006.tpc) based on IAU 1991 (Bachman, 1997) is modified to reflect this change. Three SPK kernels are encountered in this study, which are respectively prepared

by MGS NAV team, JPL Inner Planet Navigation and Gravity (IPNG) group, and NASA's Goddard Space Flight Center (GSFC) MOLA team. These kernels are compared in order to choose an appropriate one. It is found that their differences are from 0 to 50 m at maximum, mainly in the across track direction. Since the SPK kernel prepared by MGS NAV team is the closest to the average of the three, it is chosen for this study.

Calculation of the MOLA Profile

This process obtains the MOLA range measurements and the 3D coordinates of MOLA profiles on the surface of Mars. The MOLA ranges, acquisition time, and many other processing results are stored in Precision Experiment Data Records (PEDR) files prepared by NASA. MOLA footprint coordinates are embedded in the PEDR files found in the previous data preparation step. Each PEDR file contains MOLA data of approximately 12 orbits corresponding to a 32 megabyte file size (http://wufs.wustl.edu/geodata/mgs-m-mola-3-pedr-11a-v1/mgsl_21xx/aareadme.htm, last accessed 09 July 2004), and contains many columns which are not needed for downstream processing. Therefore, it is necessary to reduce the data set to a more workable size by extracting only the MOLA points that actually lie on the MOC image and only the columns necessary for further processing. Since mapping activities are using IAU 2000, whereas the MOLA files were processed based on IAU 1991 at that time, a final datum conversion from IAU 1991 to IAU 2000 is needed. A program developed by Thomas C. Duxbury at JPL is used for this conversion, which involves two steps, from IAU 1991 to the J2000 inertial coordinate system, and then from J2000 to IAU 2000. A known MOLA clock time bias of 117 ms (NAIF, 2001) needs to be corrected in this conversion. At the end, the areographic coordinates are transformed to areocentric coordinates which are then converted to Cartesian coordinates. 3D MOLA footprint coordinates calculated in this way, along with MOLA range measurements, topographic heights, and the ET time are then used as an input for photogrammetric reduction.

As the final step in data preprocessing, we need to independently verify the extraction and calculation process described above. For this purpose, the corrected MOLA ET time tag associated with each MOLA footprint is used as an index to extract the corresponding MGS position from the SPICE kernels. The distances between MOLA footprints and the corresponding MGS positions are then calculated using their 3D coordinates. These calculated distances are compared with the corresponding MOLA range measurements obtained from PEDR files. Figure 2 plots the distance differences for every MOLA profile of the study sites. Their mean and standard deviation are listed in Table 3.

Several observations can be drawn based on theses results. First, the small standard deviation values (from 0.015 m to 1.077 m) in Table 3 suggest that the uncertainty remains roughly as a constant within one MOLA profile. Second, different orbits may show quite different magnitudes of inconsistency, from 0.6 m to −25.4 m in our study sites. Most average differences are within a few (<4) meters, however, the inconsistency can rise to as large as −25 m in some MOLA profile (e.g., Isidis Planitia site, E02-01301). Referring back to the emission angles listed in Table 2, it is noticed that the inconsistency of off-nadir profiles is considerably higher than at nadir. This observation is consistent with the quality assessment of MOLA data processing reported in (Neumann, *et al.*, 2001). Third, small outliers may exist in MOLA profile. As shown in Figure 2c (E02-02016, Isidis Planitia site), differences up to 5 m, or about five times the magnitude of the standard deviation, are observed. All this inconsistency will cause certain errors in precise MOC-MOLA registration and photogrammetric reduction. However, it should be pointed out that this uncertainty is small in comparison to other error sources and resolution limit, such as the 130 m MOLA footprint resolution (Table 1).

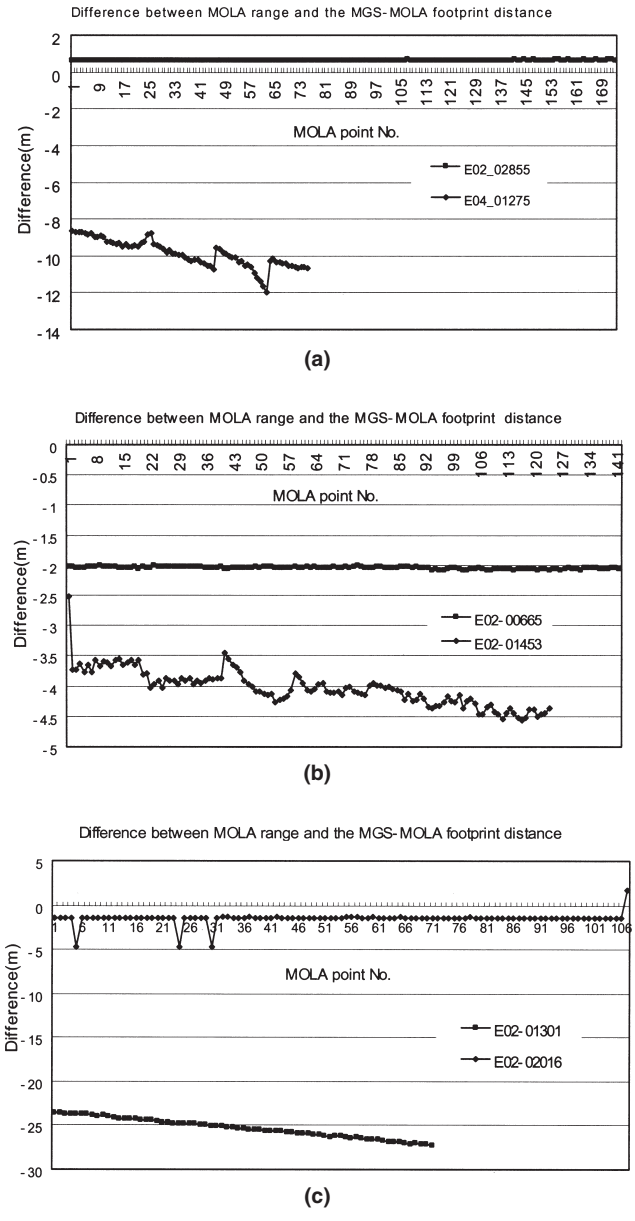

Figure 2. Differences between MOLA range measurements and the calculated MGS-MOLA footprint distances. (a) Eos Chasma. (b) Gusev Crater. (c) Isidis Planitia.

TABLE 3. COMPARISON OF MOLA RANGES AND CALCULATED MGS-MOLA FOOTPRINT DISTANCES

Site Name	Image Name	No. of MOLA Ranges	Mean (m)	Std. Dev. (m)
Eos Chasma	E02-02855	174	0.637	0.015
	E04-01275	76	−9.889	0.739
Gusev Crater	E02-00665	142	−2.044	0.019
	E02-01453	124	−4.029	0.299
Isidis Planitia	E02-01301	71	−25.359	1.077
	E02-02016	107	−1.435	0.635

Sensor Modeling

For the photogrammetric reduction of MOC images, the exterior orientation, including position and pointing, of each scan line is often treated as a function of exposure time t or the along track image coordinate x (Konecny, *et al.*, 1987; Kratky, 1989). For the convenience of computation, the origin of the x-coordinate is selected at the central scan line of a MOC image. For a second order polynomial, this model can be written as the following equations:

$$\begin{aligned} Xc(x) &= a_0 + a_1x + a_2x^2 \\ Yc(x) &= b_0 + b_1x + b_2x^2 \\ Zc(x) &= c_0 + c_1x + c_2x^2 \\ \omega(x) &= d_0 + d_1x + d_2x^2 \\ \varphi(x) &= e_0 + e_1x + e_2x^2 \\ \kappa(x) &= f_0 + f_1x + f_2x^2, \end{aligned} \tag{2}$$

where $Xc(x)$, $Yc(x)$, $Zc(x)$ are the ground coordinates of the exposure center of the MOC scan line x; $\omega(x)$, $\varphi(x)$, $\kappa(x)$ are the pointing angles of the MOC scan line x; $a_0 \ldots f_2$ are the polynomial coefficients of the corresponding sensor parameters. The task of sensor modeling is essentially to use various satellite trajectory data stored in the SPICE kernels to determine these polynomial coefficients. Considering the fact that a MOC image is taken in a very short orbital path (usually about 12 seconds), our study uses only the first and the second order polynomials to model the sensor movement and orientation.

The modeling process includes the following steps. First, the scanning start time of a MOC image, exposure time per scan line, and the number of scan lines (see Table 2) are obtained from the MOC image header file. The entire acquisition time period of a MOC image is then equally divided into 30 intervals. The time instants at these intervals will be used as an index to extract and calculate the MOC scan line's positions and pointing from the SPICE kernels as previously described. For each MOC image, positions and pointing are calculated at these equally spaced time intervals. These values will then be used in Equation 2 to determine the polynomial coefficients based on the least squares criterion.

To examine the behavior of the MOC pointing and position change, Table 4 lists the root mean square error (RMSE) of modeling computation using the first and second order polynomials. The RMSE is under the areocentric coordinate system (IAU, 2000) where the computation is carried out. To illustrate the sensor modeling behavior, Figure 3 plots the residuals for the two images over the Eos Chasma site. As is shown, the first order polynomial modeling yields relatively large residuals for both MOC positions and pointing. The residuals can be as large as 29 m for position and seven arc seconds for pointing. The use of the second order polynomial can significantly improve the precision for sensor modeling, even though the corresponding orbit during the exposure period is relatively very short (about 12 seconds). The residuals are reduced to a magnitude of millimeters for position and a maximum of five arc seconds (equivalent to approximately 9 m on the ground in position) for pointing. It should be noted that the improvement on pointing using the second order polynomial is generally limited (approximately 30–40 percent) compared to the improvement on positions. A higher order polynomial may further reduce the residuals for MOC pointing. However, the complicated shape of pointing residuals in Figure 3 suggests that this will not completely eliminate modeling errors. For the rest of the paper, we use the second order polynomial to model the sensor, and conduct MOC-MOLA registration and 3D point determination.

Registration of MOLA Profile to MOC Stereo Images

Principle

The purpose of MOLA and MOC registration is to determine the location of MOLA footprints on one or more MOC images that cover the same area. In this way, every MOLA point can then be properly weighed as a control point for the subsequent MOC photogrammetric processing. In addition, if one MOLA footprint can be independently registered onto two or more corresponding MOC images, a comparison of the image features of these corresponding registrations will reveal the registration uncertainty. The registration is conducted by using the collinearity equations (Wang, 1990, pp. 3–5; Wolf and Dewitt, 2000, Chapter 11):

$$\begin{aligned} x &= -f\,\frac{m_{11}(X - Xc) + m_{12}(Y - Yc) + m_{13}(Z - Zc)}{m_{31}(X - Xc) + m_{32}(Y - Yc) + m_{33}(Z - Zc)} \\ y &= -f\,\frac{m_{21}(X - Xc) + m_{22}(Y - Yc) + m_{23}(Z - Zc)}{m_{31}(X - Xc) + m_{32}(Y - Yc) + m_{33}(Z - Zc)}, \end{aligned} \tag{3}$$

where

(X, Y, Z) are the ground coordinates of a MOLA footprint;

(x, y) are the image coordinates of a MOLA footprint, with x along the flight direction;

TABLE 4. RMSE OF 1ST AND 2ND ORDER POLYNOMIAL SENSOR MODELING

Site	Image Name	Polynomial Order	Position RMSE (meters)			Pointing RMSE (seconds)		
			X_c	Y_c	Z_c	ω	φ	κ
Eos Chasma	E02-02855	1	29.035	23.662	8.762	2.706	1.907	4.056
		2	0.001	0.019	0.051	1.758	1.622	2.347
	E04-01275	1	8.339	7.389	2.639	0.380	1.182	1.048
		2	0.0003	0.003	0.008	0.379	1.179	1.045
Gusev Crater	E02-00665	1	26.998	0.716	7.051	7.221	4.229	6.495
		2	0.007	0.010	0.031	5.028	3.470	4.169
	E02-01453	1	19.697	0.299	5.078	3.829	2.238	4.059
		2	0.005	0.006	0.020	3.072	1.598	4.034
Isidis Planitia	E02-01301	1	0.749	7.285	2.776	0.388	0.845	0.855
		2	0.288	0.193	2.256	0.170	0.846	0.588
	E02-02016	1	1.693	16.525	1.537	3.231	0.874	1.673
		2	0.049	0.035	0.382	1.226	0.478	0.473

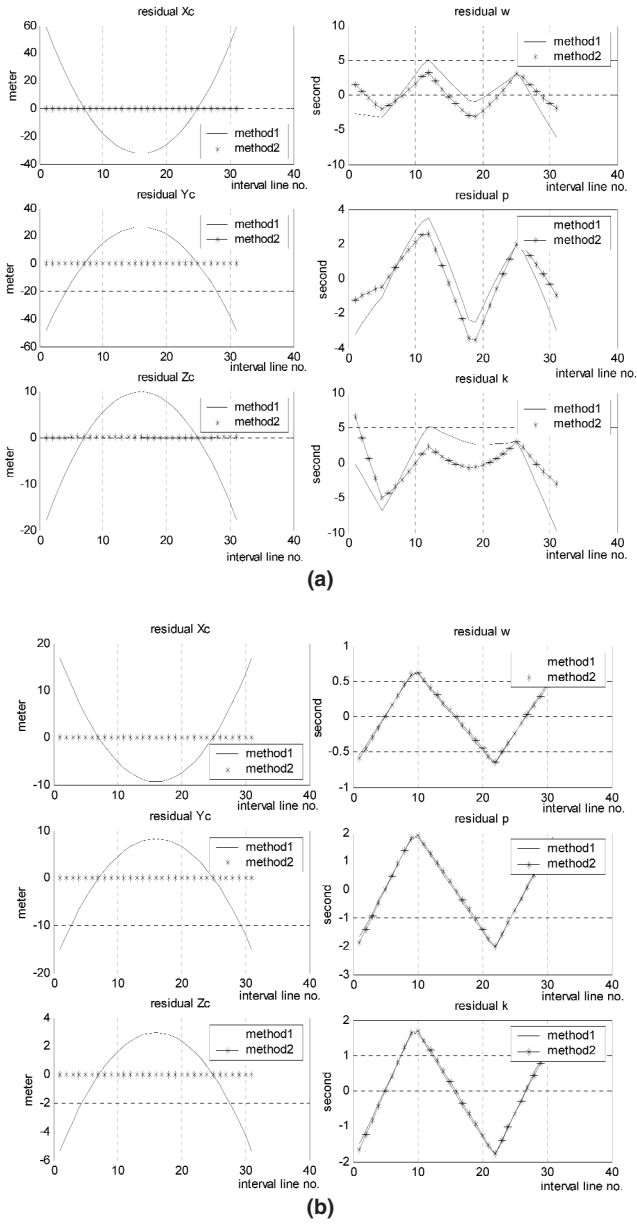

Figure 3. Residuals at scan lines after sensor modeling. (a) E02-02855 (b) E04-01275 (Eos Chasma site. $w = \omega$, $p = \varphi$, $k = \kappa$. Method 1 and 2 are respectively for the first and second order polynomials. One MOC image is equally divided to 30 intervals as shown in the horizontal axis.)

(Xc, Yc, Zc) are the ground coordinates of the MOC exposure position;

$m_{11}, \ldots m_{33}$ are the elements of the rotation matrix formed by the exterior orientation parameters;

f is the focal length of MOC.

Equation 3 is a general form of the collinearity condition. If the exterior orientation parameters, namely, $m_{11}, \ldots m_{33}$ and (Xc, Yc, Zc), are treated as time-independent, then it is the same as the relationship for a frame camera; otherwise, if the sensor model Equation 2 is used, it is for a pushbroom camera such as MOC, and the x-coordinate will become zero.

An iterative approach (Konecny, *et al.*, 1987; Wang, 1990, pp. 529–531) is first used to project a MOLA footprint onto the MOC images using the collinearity equations. For completeness and the convenience of readers, this approach is briefly summarized as follows. For each MOLA footprint, MOC image is first treated as a frame image with time-independent exterior orientation parameters. This set of parameters is taken from the central scan line of the MOC image, namely the a_0, $b_0 \ldots$ and f_0 coefficients in Equation 2. The corresponding projection of a MOLA footprint on the MOC image is then calculated with Equation 3 using this initial exterior orientation. Next, the calculated x coordinate along the flight direction is used to update the exterior orientation with Equation 2. After this step, the updated time-dependent exterior orientation is used to calculate the image coordinate correction $dx = x$ with Equation 3. This process stops once the correction dx approaches zero. The calculation steps are shown below:

Step 1. Let $X_c = X_c(0)$, $Y_c = Y_c(0)$, $Z_c = Z_c(0)$, $\omega = \omega(0)$, $\varphi = \varphi(0)$, $\kappa = \kappa(0)$, where "0" denotes the time at the central scan line.

Step 2. Calculate (x, y) coordinates using the collinearity Equation 3.

Step 3. Calculate the exterior orientation parameters for each scan line using Equation 2.

Step 4. Use Equation 3 to calculate the x coordinate correction (dx) with the updated orientation parameters.

Step 5. Update the x approximate coordinate $x\_new = x\_old + dx$. If dx is beyond a given tolerance, return to Step 3; otherwise the iteration terminates.

Our experience shows that the above approach converges slowly and is vulnerable to the initial values. A new iterative algorithm is developed as follows. When the correct exterior orientation parameters are used for one scan line, the first equation of the collinearity condition in Equation 3 should be zero, namely:

$$m_{11}(X - X_c) + m_{12}(Y - Y_c) + m_{13}(Z - Z_c) = 0.$$

Inserting the sensor modeling of camera position in Equation 2 to the above equation and rearranging its terms will lead to

$$(m_{11}a_1 + m_{12}b_1 + m_{13}c_1)x = m_{11}(X - a_0 - a_2x^2) + m_{12}(Y - b_0 - b_2x^2) + m_{13}(Z - c_0 - c_2x^2).$$

The new iteration algorithm is then based on the following equation:

$$x_{i+1} = \frac{m_{11}\left(X - a_0 - a_2x_i^2\right) + m_{12}\left(Y - b_0 - b_2x_i^2\right) + m_{13}\left(Z - c_0 - c_2x_i^2\right)}{(m_{11}a_1 + m_{12}b_1 + m_{13}c_1)}, \quad (4)$$

where x_i and x_{i+1} are the x coordinates at the i-th and $(i + 1)$-th iterations, respectively. The iteration starts with x_0 calculated by treating the MOC image as a frame image. For each iteration, the current scan line coordinate x_i will be used to calculate a new set of exterior orientation parameters using the sensor model in Equation 2. The calculation stops when the difference of x coordinates $|x_{i+1} - x_i|$ in two consecutive iterations is smaller than a given tolerance. Once the scan line location x is determined, the y coordinate can be calculated with the second equation of the collinearity condition in Equation 3.

Performance

Tests are carried out to compare the performance of the new algorithm with the relationship presented by Konecny, *et al.*, 1987, and Wang, 1990, pp. 529–531. For a given convergence

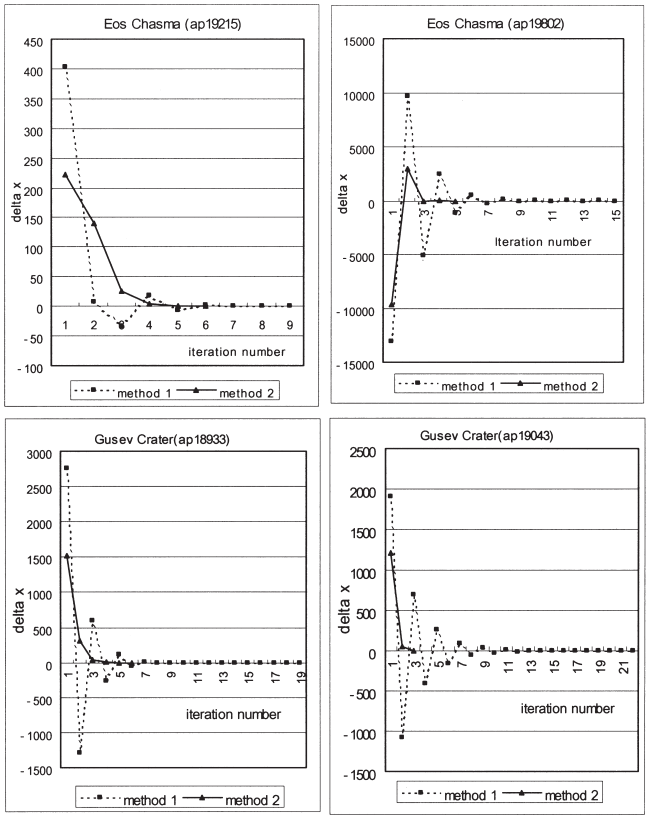

Figure 4. Convergence of the two algorithms for MOC-MOLA registration. (Solid line: proposed approach; dash line: existing approach in Konecny *et al.*, 1987, Wang, 1990. The horizontal axis is the number of iterations, the vertical axis is average $(x_{i+1} - x_i)$ in pixels.)

tolerance of 0.1 pixels, the number of iterations needed for each MOLA footprint is counted. The average number of iterations for all the MOLA footprints (the total number of iterations divided by the total number of MOLA footprints) is used as the evaluation criterion. To register the 174 MOLA points to the two images in Eos Chasma site, the new algorithm needs an average of 2.9 iterations as opposed to 13.6 iterations needed for the existing algorithm. Another test using Gusev Crater data set suggests the similar conclusion. 142 MOLA points are projected to Gusev Crater E02-00665 image. The new algorithm needs an average of 5.6 iterations, while the existing one takes 17.1 iterations. In addition, our tests show that the new algorithm is robust to the selection of initial values. To illustrate the convergence behavior, Figure 4 plots the average of the difference $(x_{i+1} - x_i)$ for all the points at each iteration. Clearly, the new algorithm (labeled as method 2 in Figure 4) converges about 3–4 times, depending on the images, more rapidly than the existing one (labeled as method 1 in Figure 4). Finally, it should be noted that projecting a ground point onto the images is a general problem for mapping with images collected from pushbroom sensors. The new algorithm proposed here can also be used for other related mapping applications.

Registration

Based on the MOLA footprint coordinates calculated before and the above proposed registration approach, a MOLA profile can be projected to MOC images over the same area. As shown in Table 2, for every study site there are two images and two MOLA profiles. We project every MOLA profile onto the two images, of which one was collected simultaneously with the MOLA data, while the other was collected at a different time from a different orbit. As a result of this, for every study site two projected profiles are overlaid atop the two MOC images as shown in Figure 5. MOLA footprint (relative sequential) numbers are labeled beside each MOLA point location. The average ground and image distances of two adjacent MOLA points are also labeled on the images to provide scale information for interpretation and analysis.

Figure 5 reveals some important properties of the MGS mapping data. First, the projection of a MOLA profile is nearly a straight line on the MOC images. This straight line is parallel to the flight direction and offset from the center of the image scan line. The offset verifies the MOC and MOLA instrument boresight difference which is documented in the SPICE kernels and considered in the ISIS package in the registration of MOLA profile to MOC images (Kirk, *et al.*, 2001). Second, a visual check by using the common image features as a reference indicates that the two projections of the same MOLA point on two images are inconsistent at the magnitude of one MOLA GSD (averaging 325 m) along the flight direction, which corresponds to 55 to 104 pixels on the images depending on the image scale. For example, at the Eos Chasma site, point 74 of MOLA profile "ap19215" (left profile on the images) on the left image is projected at approximately the same location as point 73 of the same profile on the other image. A similar observation can be made for point 109 on the left image and 108 on the right image for MOLA profile "ap18933" of the Gusev Crater site. Such a comparison can be made for all six MOLA profile pairs in all six images. It verifies that the uncertainty of the two projections of one MOLA point on two images is about one MOLA GSD, which is the MOC-MOLA registration uncertainty, if no additional correction is applied. Third, it is noted that the registration uncertainty remains more or less the same over one image regardless the point location on the image. This uncertainty behavior in MOC-MOLA registration suggests a possible constant bias in determining the exposure time instant of scan lines. Detailed uncertainty analyses are presented in the next two sections.

The proposed registration approach has several distinctions. First, the registration process is conducted using the 3D MOLA coordinates derived from PEDR files. Once their corresponding locations on the MOC images are determined, MOLA points can then be properly weighed as ground control for subsequent photogrammetric processing. Another distinction is that no calibration knowledge on MOLA and MOC relative orientation is needed in this process. Third, by using this approach multiple MOLA profiles can be registered to stereo or multiple images. As is addressed above, this provides an independent check on the registration uncertainty by comparing the image features of MOLA projections. All these are made possible by the use of the 3D MOLA coordinates and rigorous photogrammetric geometry. Since all the computation is based on the collinearity condition, it can be modified by including additional parameters to refine the current MOC-MOLA registration results and calibrate the MOC-MOLA relative orientation.

Ground Point Determination

The determination of ground point 3D position is crucial for generating control network and DEM. In this section, the two images for each study site are used to determine the 3D ground coordinates of image points. During this process, the sensor model parameters are treated as known, while image measurements are treated as observations. This is a standard, but not necessarily an optimal treatment. However, it is appropriate for studying the uncertainty of ground point determination caused by the sensor modeling errors, and sufficient at this point to understand the mapping capabilities of the MGS data.

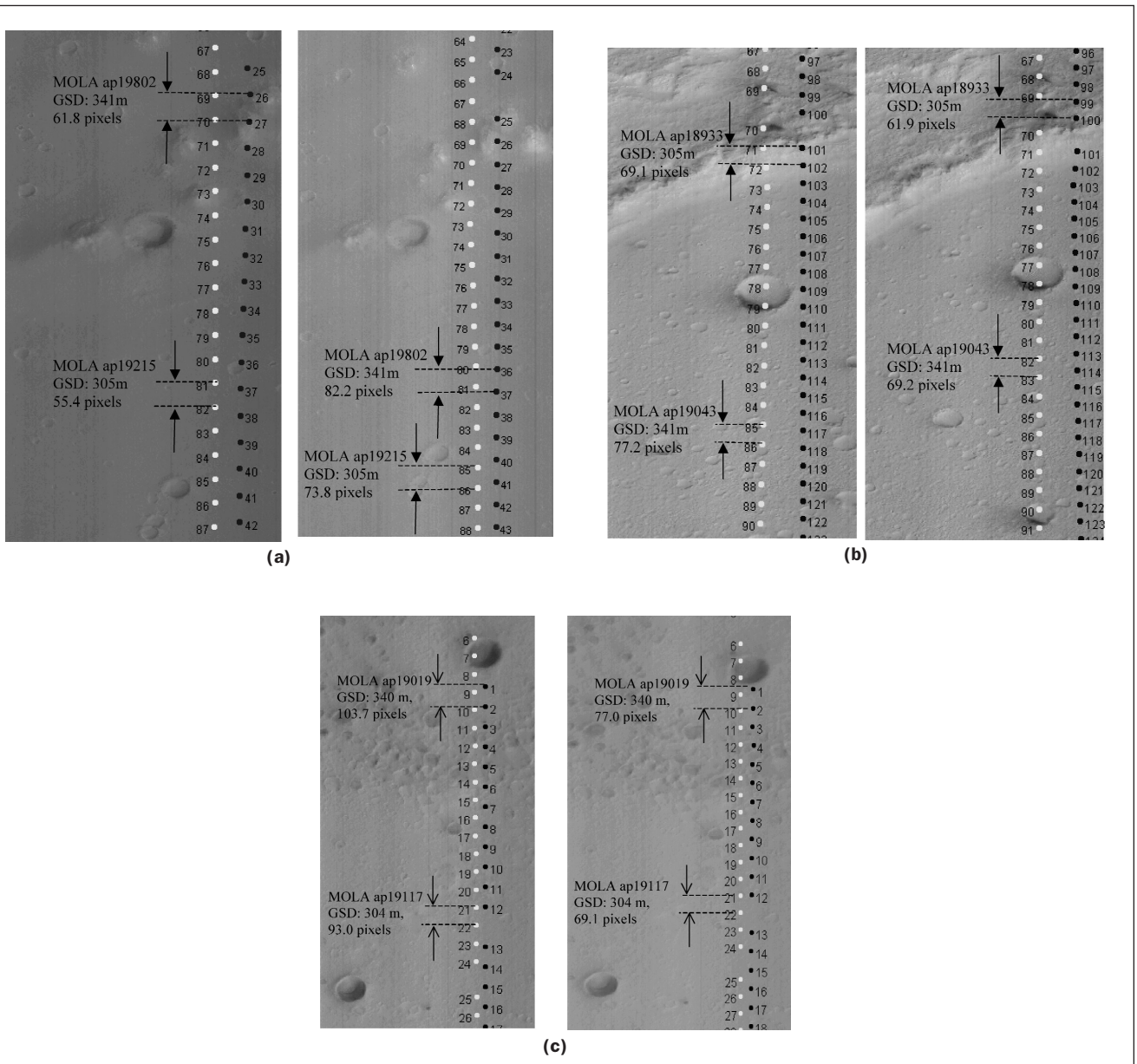

Figure 5. MOLA profiles registered on stereo pairs. (A vertical portion of the image is shown with south pointing up. The flight direction is from south to north. The labeled numbers are relative sequential MOLA point numbers. One MOLA profile is projected on the two images in the stereo pair. The average ground spacing distance (GSD) and image distance in pixels of two adjacent MOLA points are labeled on each image to provide approximate scale information.)
(a) Eos Chasma. Left: E02-02855; Right: E04-01275. (b) Gusev Crater. Left: E02-00665; Right: E02-01453.
(c) Isidis Planitia. Left: E02-01301; Right: E02-02016.

The calculation is based on the intersection of two sets of collinearity equations, one for each image in the stereo pair. Equation 3 is linearized by treating ground coordinates X, Y, Z as unknown, exterior orientation parameters as known, and image coordinates as observations. For each ground point, four equations are obtained and the least squares criterion is used to find out the solution. The detailed linearization procedure and calculation steps are similar to the descriptions in (Wolf and Dewitt, 2000, pp. 245–246 and pp. 554–556; Wang, 1990, Chapter 2), where the formulas are given for images obtained from a frame camera which are generalized for pushbroom images in this work.

The 3D ground coordinates of a number of image points are determined through intersection calculation based on their measurements in the stereo pair. Image measurements are obtained by the combination of manual and automatic measurement. First, about 24 points are manually measured in a stereo pair. These manual measurements are then used as *seed points* in a commercial photogrammetric tool (IMAGINE OrthoBASE® Pro 8.5.1) to automatically collect more points. The total number of points collected in each stereo pair is listed in Table 5. Difficulty is encountered in this measurement process due to the low image contrast, different resampling factor, image scale, and ground reflection. A visual check on these measurements suggests that the accuracy is better than two pixels. For every image measurement, image residuals can be calculated which indicate how well the two conjugate projection lines intersect. Their respective

TABLE 5. STATISTICS OF INTERSECTION RESIDUALS (IN PIXELS)

Site Name	No. of Points	Image 1				Image 2			
		M_x	σ_x	M_y	σ_y	M_x	σ_x	M_y	σ_y
Eos Chasma	162	−33.82	17.34	2.86	1.36	20.52	10.17	−1.61	0.76
Gusev Crater	154	−26.25	0.66	3.63	0.27	23.55	0.59	−2.62	0.23
Isidis Planitia	41	34.29	0.96	−2.57	0.22	−25.48	0.72	2.88	0.24

where M_x, M_y: means of residuals in x and y coordinates, in pixels.
σ_x, σ_y: standard deviation of residuals in x and y coordinates, in pixels.

means and standard deviations are listed in Table 5, where column Image 1 and 2 are corresponding to the Image Number in Table 2. To examine the distribution of the residuals, the residual vectors at each image point are plotted in Figure 6, where the flight direction is from left (south) to right (north).

A few conclusions can be drawn from Table 5 and Figure 6. First, the intersection uncertainty occurs mainly in the flight direction (x). The x-residuals can be as high as 51 pixels (1σ, Eos Chasma site), whereas the y-residuals are only about 4 pixels (1σ, Eos Chasma site). This observation is consistent with the MOC-MOLA profile registration shown in Figure 5.

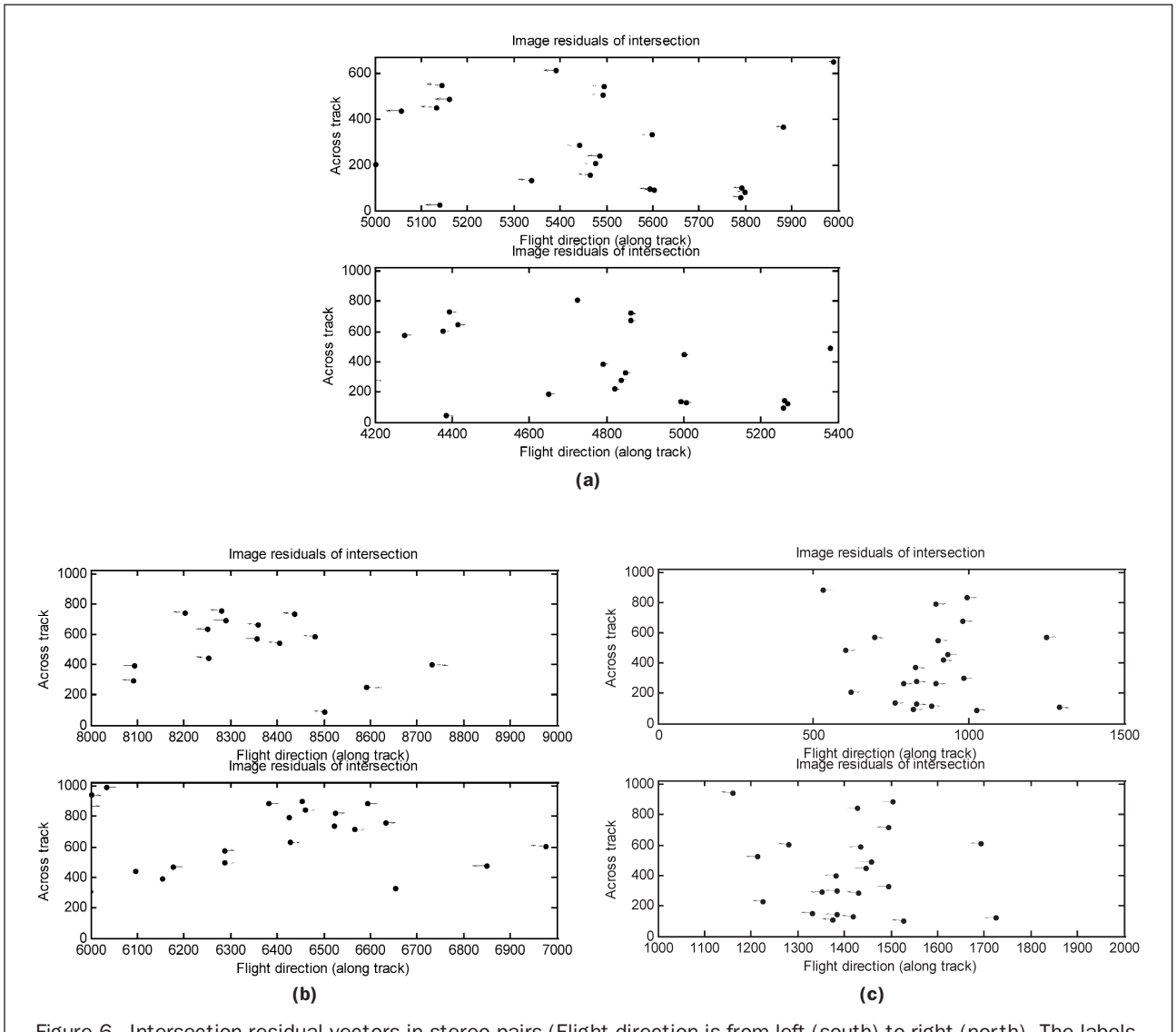

Figure 6. Intersection residual vectors in stereo pairs (Flight direction is from left (south) to right (north). The labels in the horizontal direction are line number, while the labels in the vertical direction are the pixel numbers in a scan line. Only a portion of the images is shown. The total dimension of the images is listed in Table 2.)
(a) Eos Chasma. Top: E02-02855; Bottom: E04-01275 (b) Gusev Crater. Top: E02-00665; Bottom: E02-01453
(c) Isidis Planitia. Top: E02-01301; Bottom: E02-02016.

Second, the very small standard deviation values (less than 1 pixel except for Eos Chasma site) in the x direction again suggest the same conclusion obtained from the MOC-MOLA registration that a constant uncertainty exists along the flight direction. This uncertainty may be corrected by introducing additional parameters for every MOC image and MOLA profile. Third, the means of the residuals for the two images in a stereo pair have opposite signs with similar magnitudes which suggests that the SPICE kernel uncertainties are well balanced by the least squares adjustment among the two images. The plots in Figure 6 also suggest the similar magnitudes of residuals with opposite signs in the two images of a stereo pair. Finally, the two images of Eos Chasma site present considerably larger standard deviation (approximately 17 and 10 pixels for left and right images, respectively) than the other two study sites. This is probably because of the large span of acquisition dates for the two images. As shown in Table 2, they were respectively collected on 31 March 2001 and 18 May 2001 which correspond to two mission extension periods. For this reason, two different sets of SPICE kernels need to be used to calculate the exterior orientations. For the other two study sites, the stereo pairs were acquired within less than 10 days in the same mission period, and the same SPICE kernels are used. This fact implies that different sets of SPICE kernels for different mission periods may have considerable inconsistencies.

Uncertainty Analysis

Based on the intersection results in Table 5 and the results obtained in MOC-MOLA registration, we are now able to separately estimate the uncertainties of the SPICE kernels, MOLA data, and MGS mapping products. The discrepancy of the two projections of one ground point on two images can be written as

$$\begin{aligned} \Delta x &= \Delta x_1 - \Delta x_2 \\ \Delta y &= \Delta y_1 - \Delta y_2 \end{aligned}, \tag{5}$$

where x_1, y_1 and x_2, y_2 are the image coordinates of a ground point respectively on the two images, Δ denotes the discrepancy. The ground point can be either a MOLA point or a point determined using the intersection calculation. Since the uncertainty across track (y-direction) is at the level of image measurement errors, only the uncertainty along the flight direction will be considered. The total discrepancy Δx consists of two parts, the one caused by the exterior orientation (SPICE kernels) errors and the one caused by ground point errors. Namely, we have the following uncertainty relationship

$$D^2_{\Delta x} = D^2_{\Delta x}(EO) + D^2_{\Delta x}(G), \tag{6}$$

where $D_{\Delta x}(EO)$ is the uncertainty caused by the SPICE kernels or exterior orientation; $D_{\Delta x}(G)$ is the uncertainty contributed from the ground point, all counted at image scale and along flight direction.

First, we estimate the uncertainty of the exterior orientation $D_{\Delta x}(EO)$ in Equation 6. Since for intersection calculation $D_{\Delta x}(G)$ is equal to zero, the SPICE kernels are the only error source if the small image measurement errors are ignored. The intersection errors listed in Table 5 is predominately caused by the uncertainty of SPICE kernels, or to be more specific, by the uncertainty of exterior orientation. To estimate $D_{\Delta x}(EO)$, we first calculate the uncertainty $D^2_x = M^2_x + \sigma^2_x$ for each image in Table 5 and take the average for the left and right images, respectively. Thus we obtain the uncertainty of exterior orientation as follows

$$D^2_{\Delta x}(EO) = D^2_{x1} + D^2_{x2}. \tag{7}$$

Based on the values in Table 5, this calculation yields $D_{\Delta x}(EO) = 41.0$ pixels, which is the uncertainty estimation for the exterior orientation at image scale.

Second, we estimate the uncertainty of MOLA points determined through geophysical processing. Let the ground point in Equation 6 be a MOLA point, then Δx is the MOC-MOLA registration error which is estimated as one MOLA GSD as shown in Figure 5. Taking the average GSD listed in Table 2, we obtain $D_{\Delta x} = 74.0$ pixels. Inserting this and $D_{\Delta x}(EO) = 41.0$ pixels into Equation 6, we can then estimate the uncertainty of the MOLA data as $D_{\Delta x}(MOLA) = 61.6$ pixels.

Finally, we estimate the photogrammetric mapping uncertainty. The uncertainty of planimetric distance D_P depends on the error of exterior orientation. This can be represented as

$$D_P = \sqrt{D^2_{\Delta x}(EO) + D^2_{\Delta y}(EO)}, \tag{8}$$

where $D_{\Delta x}(EO)$ and $D_{\Delta y}(EO)$ are the uncertainties caused by the exterior orientation respectively along and across the flight directions. Based on the values in Table 5, the planimetric distance uncertainty is estimated as $D_P = \sqrt{41.0^2 + 2.8^2} = 41.1$ pixels, or 180.8 m given the average pixel size being 4.4 m in this study.

For the uncertainty of elevation difference, it depends on the altitude-base ratio and the uncertainty of the across track parallax. The relationship can be written as (Wolf and Dewitt, 2000, pp. 178–179)

$$D_h = \frac{H}{B} D_{\Delta p} = \frac{H}{B} D_{\Delta y}(EO), \tag{9}$$

where D_h is the uncertainty of the estimated elevation difference, H is the MGS altitude above ground, B is the distance between two camera stations across track, and $D_{\Delta p}$ is the uncertainty of across track parallax difference which is equal to the Δy uncertainty caused by the SPICE kernel errors. Let $H = 385$ km, $B = 155$ km calculated from this study, and $D_{\Delta y} = 2.8$ pixels in Equation 9, we obtain $D_h = 7.0$ pixels. Given the average MOC image-ground resolution as 4.4 m per pixel, the elevation difference uncertainty is then estimated as 30.8 m.

Conclusions

Accessing and understanding the MGS data is essential for photogrammetric processing. Through an exhaustive search, we are able to find all the corresponding MOLA data, including points both simultaneously and non-simultaneously collected with a MOC image. During the data preparation and preprocessing process, care is needed to ensure that data from a variety of sources are obtained correctly, consistently, and transformed to one common coordinate system. An independent check is necessary to validate this process and helpful to evaluate the final outcome. The distances between the MOLA range measurements and the distances calculated using MGS positions and MOLA footprints are found to be nearly a constant within one MOLA profile and may vary from profile to profile. Considerably larger discrepancies of up to 25 m in off-nadir profiles are observed than in nadir profiles (approximately 5 m).

The proposed MOC-MOLA registration approach is able to handle both simultaneously and non-simultaneously collected MOLA data. It can register a MOLA profile to the two stereo MOC images over the same area. The new iterative algorithm for projecting a MOLA point onto a MOC image is robust to initial values and converges about 3 to 4 times faster than the existing algorithm. The MOC-MOLA registration uncertainty is found to be nearly a constant of one MOLA GSD (approximately 325 m) along the flight direction. This suggests a possible constant bias in determining the exposure time instant of scan lines.

Uncertainty exists in all data sources and the photogrammetric mapping process. It is shown, if counted at image scale, the uncertainty of MOLA point is 61.6 pixels. The SPICE kernels have an uncertainty of 41.1 pixels for planimetric distance and 7.0 pixels for elevation difference, which correspond to 180.8 m and 30.8 m, respectively, given the average pixel size being 4.4 m on the ground and the altitude-base ratio being 2.5 in this study.

In future studies, additional parameters and measurements will be introduced along with multiple (>2) MOLA profiles and multiple (>2) MOC images to correct the constant uncertainty in MOC-MOLA registration so that only the random errors in SPICE kernels may affect the final mapping outcome.

Acknowledgments

This work is sponsored by the National Aeronautics and Space Administration (NASA).

References

Acton, C., 1996. Ancillary Data Services of NASA's Navigation and Ancillary Information Facility, *Planetary and Space Science*, 44, pp. 65–70.

Albee, A.L., R.E. Arvidson, F. Palluconi, and T. Thorpe, 2001. Overview of the Mars Global Surveyor mission, *Journal of Geophysical Research*, Vol. 106, No. E10, October 25, pp. 23,291–23,316.

Anderson, F.S., and T.J. Parker, 2002. Characterization of MER landing sites using MOC and MOLA, *Abstract 2028*, The 33rd Lunar and Planetary Science Conference, March 11–15, League City, Texas.

Archinal, B.A., T.R. Colvin, M.E. Davies, R.L. Kirk, T.C. Duxbury, E.M. Lee, D. Cook, and A.R. Gitlin, 2002. MOLA-controlled RAND-USGS control network for Mars, *Abstract 1632*, The 33rd Lunar and Planetary Science Conference, March 11–15, League City, Texas.

Bachman, N., 1997. PCK required reading, *NASA, NAIF*, URL: ftp://naif.jpl.nasa.gov/pub/naif/MGS/kernels/pck/, last accessed 09 July 2004.

Baratoux, D., C. Delacourt, and P. Allemand, 2001. New local DEM derived from combination of high-resolution Viking Images and the high-precision MOLA data set, *Abstract 1305*, The 32nd Lunar and Planetary Science Conference, Huston, Texas.

Beyer, R.A., and A.S. McEwen, 2002. Photoclinometry measurements of Meter-Scale Slopes for the Potential Landing Sites of the 2003 Mars Exploration Rovers, *Abstract 1443*, The 33rd Lunar and Planetary Science Conference, March 11–15, League City, Texas.

Caplinger, M.A., and M.C. Malin, 2001. Mars Orbiter Camera geodesy campaign, *Journal of Geophysical Research*, Vol. 106, No. E10, October 25, pp. 23,595–23,606.

Caplinger, M.A., 2002. Mars orbiter camera global mosaic, *Abstract 1405*, The 33rd Lunar and Planetary Science Conference, March 11–15, League City, Texas.

Davies, M., T. Colvin, R.L. Kirk, E. Lee, and R. Sucharski, 1999. Status of the RAND-USGS control network of Mars, *Second Workshop on Mapping of Mars and ISPRS WG IV/5 Extraterrestrial Mapping Workshop, Proceedings*, July 23–24, California Institute of Technology, Pasadena, California, USA.

Duxbury, T.C., R.L. Kirk, B.A. Archinal, and G.A. Neumann, 2002. Mars Geodesy/Cartography working group recommendations on Mars cartographic constants and coordinate Systems, *IAPRS,* Vol. 34, Part 4, "Geospatial Theory, Processing and Applications," Ottawa, 8–12 July, unpaginated CD-ROM.

Ivanov, A.B., and J.J. Lorre, 2002. Analysis of Mars Orbiter camera stereo pairs, *Abstract 1845*, The 33rd Lunar and Planetary Science Conference, March 11–15, League City, Texas.

Kim, J.-R., J.P. Muller, and J.G. Morley, 2000. Towards Automated MOLA track registration in MOC and Viking Images and its application to the establishment of new 3-D control point network on Mars, *ISPRS Congress Proceedings*, Amsterdam, The Netherlands, July 16–22, unpaginated CD-ROM.

Kirk, R.L., E. Howington-Kraus, and M. Rosiek, 2000. Recent planetary topographic mapping at the USGS, Flagstaff: Moon, Mars, Venus, and beyond, *IAPRS*, Vol. 33, Part B4, pp. 476–490.

Kirk, R.L., T.L. Becker, E.M. Eliason, J. Anderson, and L.A. Soderblom, 2001. Geometric calibration of the Mars orbiter cameras and coalignment with Mars orbiter laser altimeter, *Abstract 1863*, The 32nd Lunar and Planetary Science Conference, Huston, Texas.

Kirk, R.L., E. Howington-Kraus, and B.A. Archinal, 2002a. Topographic Analysis of Candidate Mars Exploration Rover Landing Sites from MOC Narrow Angle Stereoimages, *Abstract 1988*, The 33rd Lunar and Planetary Science Conference, March 11–15, 2002, League City, Texas.

Kirk, R.L., L.A. Soderblom, E. Howington-Kraus, and B. Archinal, 2002b. High resolution topomapping of Mars with Mars Orbiter Camera Narrow-angle Images, *IAPRS*, Vol. 34, Part 4, "Geospatial Theory, Processing and Applications," Ottawa, unpaginated CD-ROM.

Konecny, G., P. Lohmann, H. Engel, and E. Kruck, 1987. Evaluation of SPOT imagery on analytical photogrammetric instruments, *Photogrammetric Engineering & Remote Sensing*, Vol. 53, No. 9, pp. 1223–1230.

Kratky, V., 1989. Rigorous photogrammetric processing of SPOT images at CCM Canada, *ISPRS Journal of Photogrammetry and Remote Sensing*, No. 44, pp. 53–71.

Malin, M.C., and S.K. Edgett, 2001. Mars Global Surveyor Orbiter Camera: Interplanetary cruise through primary mission, *Journal of Geophysical Research*, Vol. 106, No. E10, October 25, pp. 23,429–23,570.

Muller, J.-P, and J.-R. Kim, 1999. Assessment of published Viking Orbiter DEMs derived from stereo photogrammetry using MOLA data, *Second Workshop on Mapping of Mars and ISPRS WG IV/5 Extraterrestrial Mapping Workshop Proceedings*, July 23–24, California Institute of Technology, Pasadena, California, USA.

NAIF (Navigation and Ancillary Information Facility), 2001. MOLA Instrument Kernel Version 2.6, *NASA, NAIF*, URL: ftp://naif.jpl.nasa.gov/pub/naif/MGS/kernels/ik/, last accessed 09 July 2004.

Neumann, G., F. Lemoine, D. Rowlands, D.E. Smith, and M.T. Zuber, 2001. Crossover analysis in MOLA data processing, *Journal of Geophysical Research*, Vol. 106, No. E10, pp. 23,753–23,768.

Niedermaier, G., M. Wählisch, S. van Gasselt, F. Scholten, F. Wewel, T. Roatsch, K.D. Matz, and R. Jaumann, 2002. A Topographic Image Map of the MC-18 Quadrangle "Coprates" at 1:2000000 using Data obtained from the Mars Orbiter Camera and the Mars Orbiter Laser Altimeter of Mars Global Surveyor, *Abstract 1529*, The 33rd Lunar and Planetary Science Conference, March 11–15, League City, Texas.

Rosiek, M.R., R. Kirk, and E. Howington-Kraus, 2001. Mars Orbiter large-scale topographic Maps, *Abstract 1950*, The 32nd Lunar and Planetary Science Conference, Huston, Texas.

Seidelmann, P.K., V.K. Abalakin, M. Bursa, M.E. Davies, C. Debergh, J.H. Lieske, J. Oberst, J.L. Simon, E.M. Standish, P. Stooke and P.C. Thomas, 2002. Report of the IAU/IAG working group on cartographic coordinates and rotational elements of the planets and satellites: 2000, *Celestial Mechanics and Dynamical Astronomy*, Vol. 82, pp. 83–110.

Shan, J., D.S. Lee, and J.-S. Yoon, 2002. Photogrammetric Registration of MOC imagery with MOLA data, *Joint International Symposium on Geospatial Theory, Processing and Applications Proceedings*, Ottawa, Canada, 8–12 July, unpaginated CD-ROM.

Smith, D.E., M.T. Zuber, H.V. Frey, J.B. Garvin, J.W. Head, D.O. Muhleman, G.H. Pettengill, R.J. Phillips, S.C. Solomon, H.J. Zwally, W.B. Banerdt, and T.C. Duxbury, 1998. Topography of the northern hemisphere of Mars from the Mars Orbiter Laser Altimeter, *Science*, 279, pp. 1686–1692.

Smith, D.E., M.T. Zuber, S.C. Solomon, R.J. Phillips, J.W. Head, J.B. Garvin, W.B. Banerdt, D.O. Muhleman, G.H. Pettengill, G.A. Neumann, F.G. Lemoine, J.B. Abshire, O. Aharonson, C.D. Brown, S.A. Hauck, A.B. Ivanov, P.J. McGovern, H.J. Zwally, and T.C. Duxbury, 1999. The global topography of Mars and implications for surface evolution, *Science*, 284, pp. 1495–1503.

Smith, D.E., M.T. Zuber, H.V. Frey, J.B. Garvin, J.W. Head, D.O. Muhleman, G.H. Pettengill, R.J. Phillips, S. Solomon, H.J. Zwally,

W.B. Banerdt, T.C. Duxbury, M.P. Golombek, F.G. Lemoine, G.A. Neumann, D.D. Rowlands, O. Aharonson, P.G. Ford, A.B. Ivanov, C.L. Johnson, P.J. McGovern, J.B. Abshire, R.S. Afzal, and X. Sun, 2001. Mars Orbiter Laser Altimeter: Experiment summary after the first year of global mapping of Mars, *Journal of Geophysical Research*, Vol. 106, No. E10, pp. 23,689–23,722.

Soderblom, L.A., R.L. Kirk, and K.E. Herkenhoff, 2002. Accurate fine-scale topography for the Martian south polar region from combining MOLA profiles and MOC NA images, *Abstract 1254*, The 33rd Lunar and Planetary Science Conference, March 11–15, League City, Texas.

USGS (US. Geological Survey), 2002. Integrated Software for Imagers and Spectrometers, 2.1, URL: http://astrogeology.usgs.gov/Projects/ISIS/, last accessed 08 July 2004.

Wählisch, M., G. Niedermaier, S. van Gasselt, F. Scholten, F. Wewel, T. Roatsch, K-D. Matz, and R. Jaumann, 2002. A New digital orthoimage map of the Martian western hemisphere using data obtained from the Mars orbiter Camera at a resolution of 256 pixel/deg, *Abstract 1640*, The 33rd Lunar and Planetary Science Conference, March 11–15, 2002, League City, Texas.

Wang, Z.Z., 1990. *Principles of Photogrammetry with Remote Sensing*, Press of Wuhan Technical University of Surveying and Mapping, Publishing House of Surveying and Mapping, Beijing, 575 pages.

Wolf, P.R., and B.A. Dewitt, 2000. *Elements of Photogrammetry with Applications in GIS*, 3rd Edition, McGraw Hill, Boston, New York, 608 pages.

Wu, S.C., and F.J. Schafer, 1984. Mars control network. *Technical Papers of the 50th Annual Meeting of the American Society of Photogrammetry*, Vol. 2, pp. 456–463.

Zeitler, W., and J. Oberst, 1999. The Mars Pathfinder landing site and the Viking control point network, *Journal of Geophysical Research*, Vol. 104, No. E4, pp. 8935–8941.

Zeitler, W., T. Ohlhof, and H. Ebner, 2000. Recomputation of the Global Mars control-point network, *Photogrammetric Engineering & Remote Sensing*, Vol. 66, No. 2, pp. 155–161.

(Received 08 July 2003; accepted 21 October 2003; revised 28 October 2003)